

---

# BraVE: Offline Reinforcement Learning for Discrete Combinatorial Action Spaces

---

Matthew Landers<sup>1\*</sup>, Taylor W. Killian<sup>2</sup>, Hugo Barnes<sup>1</sup>, Thomas Hartvigsen<sup>1</sup>, Afsaneh Doryab<sup>1</sup>  
<sup>1</sup>University of Virginia, <sup>2</sup>MBZUAI

## Abstract

Offline reinforcement learning in high-dimensional, discrete action spaces is challenging due to the exponential scaling of the joint action space with the number of sub-actions and the complexity of modeling sub-action dependencies. Existing methods either exhaustively evaluate the action space, making them computationally infeasible, or factorize Q-values, failing to represent joint sub-action effects. We propose **Branch Value Estimation (BraVE)**, a value-based method that uses tree-structured action traversal to evaluate a linear number of joint actions while preserving dependency structure. BraVE outperforms prior offline RL methods by up to  $20\times$  in environments with over four million actions.<sup>2</sup>

## 1 Introduction

Offline reinforcement learning (RL) enables agents to learn decision-making policies from fixed datasets, avoiding the risks and costs inherent in online exploration [21, 22]. Existing methods have shown strong performance in low-dimensional discrete settings and continuous control tasks [1, 12, 13, 15, 19, 20]. However, many real-world decisions require selecting actions from high-dimensional, discrete spaces. In healthcare, for example, practitioners must choose among thousands of possible combinations of procedures, medications, and tests at each decision point [33].

Such settings give rise to *combinatorial* action spaces, where the number of actions grows exponentially with dimensionality, scaling as  $\prod_{d=1}^N m_d$  for  $N$  sub-action dimensions. In offline reinforcement learning, this structure induces two primary challenges: evaluating and optimizing over a large, discrete action space is computationally demanding; and making accurate decisions requires modeling sub-action dependencies from fixed datasets. Standard value-based methods can, in principle, capture sub-action dependencies but require evaluating or maximizing the Q-function over the full action space, which is intractable in high-dimensional settings. Conversely, recent approaches [3, 27] factorize the Q-function under a conditional independence assumption, reducing computational cost but limiting expressivity by precluding the modeling of sub-action interactions, which are critical in many real-world domains.

We introduce **Branch Value Estimation (BraVE)**, a value-based offline RL method for combinatorial action spaces that avoids the scalability–expressivity tradeoff of prior approaches. BraVE imposes a tree structure over the action space and uses a neural network to guide traversal, evaluating only a linear number of candidate actions while preserving sub-action dependencies. To support this structured selection process, the Q-function is trained with a behavior-regularized temporal difference (TD) loss and a branch value propagation mechanism.

Our experiments show that BraVE consistently outperforms state-of-the-art baselines across a suite of challenging offline RL tasks with combinatorial action spaces containing up to 4 million discrete

---

\*mlanders@virginia.edu

<sup>2</sup>Code is available at <https://github.com/matthewlanders/BraVE>

actions. In high-dimensional environments with strong sub-action dependencies, **BraVE improves average return by up to  $20\times$  over state-of-the-art offline RL methods**. While baseline performance degrades with increasing sub-action dependencies or action space size, BraVE maintains stable performance.

Our contributions are as follows:

1. We propose a behavior-regularized TD loss that captures sub-action dependencies by evaluating complete actions rather than marginal components in combinatorial spaces.
2. We introduce **BraVE**, an offline RL method for discrete combinatorial action spaces that captures sub-action interactions and scales to high-dimensional settings via Q-guided traversal over a tree-structured action space.
3. We empirically show that BraVE outperforms state-of-the-art baselines in environments with combinatorial action spaces, maintaining high returns and stable learning as both action space size and sub-action dependencies increase.

## 2 Preliminaries

Reinforcement learning problems can be formalized as a Markov Decision Process (MDP),  $\mathcal{M} = \langle \mathcal{S}, \mathcal{A}, p, r, \gamma, \mu \rangle$  where  $\mathcal{S}$  is a set of states,  $\mathcal{A}$  is a set of actions,  $p : \mathcal{S} \times \mathcal{A} \times \mathcal{S} \rightarrow [0, 1]$  is a function that gives the probability of transitioning to state  $s'$  when action  $a$  is taken in state  $s$ ,  $r : \mathcal{S} \times \mathcal{A} \rightarrow \mathbb{R}$  is a reward function,  $\gamma \in [0, 1]$  is a discount factor, and  $\mu : \mathcal{S} \rightarrow [0, 1]$  is the distribution of initial states. A policy  $\pi : \mathcal{S} \rightarrow \mathbb{P}(\mathcal{A})$  is a distribution over actions conditioned on a state  $\pi(a | s) = \mathbb{P}[a_t = a | s_t = s]$ .

While the standard MDP formulation abstracts away the structure of actions in  $\mathcal{A}$ , we explicitly assume that the action space is combinatorial; that is,  $\mathcal{A}$  is defined as a Cartesian product of sub-action spaces. More formally,  $\mathcal{A} = \mathcal{A}_1 \times \mathcal{A}_2 \times \dots \times \mathcal{A}_N$ , where each  $\mathcal{A}_d$  is a discrete set. Consequently,  $\mathbf{a}_t$  is an  $N$ -dimensional vector wherein each component is referred to as a sub-action.

The agent’s goal is to learn a policy  $\pi^*$  that maximizes cumulative discounted returns:

$$\pi^* = \arg \max_{\pi} \mathbb{E}_{\pi} \left[ \sum_{t=0}^H \gamma^t r(s_t, a_t) \right],$$

where  $s_0 \sim \mu$ ,  $a_t \sim \pi(\cdot | s_t)$ , and  $s_{t+1} \sim p(\cdot | s_t, a_t)$ .

In offline RL, the agent learns from a static dataset of transitions  $\mathcal{B} = \{(s_t, a_t, r_t, s_{t+1})^i\}_{i=0}^Z$  generated by, possibly, a mixture of policies collectively referred to as the behavior policy  $\pi_{\beta}$ .

Like many recent offline RL methods, our work uses approximate dynamic programming to minimize temporal difference error (TD error) starting from the following loss function:

$$L(\theta) = \mathbb{E}_{\mathcal{B}} \left[ \left( r + \gamma \max_{a'} Q(s', a'; \theta^-) - Q(s, a; \theta) \right)^2 \right], \quad (1)$$

where the expectation is taken over transitions  $(s, a, r, s')$  sampled from the replay buffer  $\mathcal{B}$ .  $Q(s, a; \theta)$  is a parameterized Q-function that estimates the expected return when taking action  $a$  in state  $s$  and following the policy  $\pi$  thereafter, and  $Q(s, a; \theta^-)$  is a target network with parameters  $\theta^-$ , which is used to stabilize learning.

For out-of-distribution actions  $a'$ , Q-values can be inaccurate, often causing overestimation errors due to the maximization in Equation (1). To mitigate this effect, offline RL methods either assign lower values to these out-of-distribution actions via regularization or directly constrain the learned policy. For example, TD3+BC [13] adds a behavior cloning term to the standard TD3 [14] loss:

$$\pi = \arg \max_{\pi} \mathbb{E}_{(s,a) \sim \mathcal{B}} [\lambda Q(s, \pi(s)) - (\pi(s) - a)^2], \quad (2)$$

where  $\lambda$  is a scaling factor that controls the strength of the regularization.

More recently, implicit Q-learning (IQL) [19] used a SARSA-style TD backup and expectile loss to perform multi-step dynamic programming without evaluating out-of-sample actions:

$$L(\theta) = \mathbb{E}_{\mathcal{B}} \left[ \left( r + \gamma \max_{a' \in \Omega(s)} Q(s', a'; \theta^-) - Q(s, a; \theta) \right)^2 \right], \quad (3)$$

where  $\Omega(s) = \{a \in \mathcal{A} | \pi_{\beta}(a | s) > 0\}$  are actions in the support of the data.

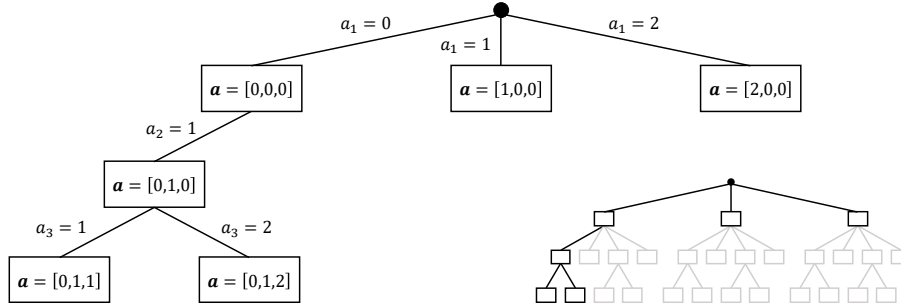


Figure 1: BraVE’s tree representation for a 3-dimensional combinatorial action  $\mathbf{a} = [a_1, a_2, a_3]$ , where each sub-action  $a_i \in \{0, 1, 2\}$ . Each node encodes a complete action vector, with explicitly chosen sub-actions set according to the traversal path from the root, and all remaining dimensions filled with a default value (here, 0). At depth  $k$ , the value of sub-action  $a_k$  is selected, with sibling nodes differing only in that dimension.

### 3 Branch Value Estimation (BraVE)

The Q-function,  $Q(s, \mathbf{a})$  in Equation (1), encodes long-term value by mapping each state–action pair to its expected return. When actions comprise multiple sub-actions  $\mathbf{a} = [a_1, \dots, a_N]$ ,  $Q(s, \mathbf{a})$  implicitly captures sub-action dependencies by accounting for interactions that influence both immediate rewards and future transitions, making it a natural target for learning in structured or combinatorial action spaces. However, in combinatorial action spaces, the exponential growth of joint actions renders both forward passes and Q-value estimation computationally intractable [30, 34].

Factorizing the Q-function across action dimensions [3, 27] is a common strategy for improving tractability. While this reduces computational cost, it sacrifices expressivity by ignoring sub-action dependencies, leading to estimation errors when sub-actions jointly influence transitions or rewards. In such settings, including real-world domains like treatment recommendation, summing marginal Q-values can produce divergent estimates (Appendix A).

We introduce **Branch Value Estimation (BraVE)**, an offline RL method that avoids this scalability–expressivity tradeoff. BraVE assigns values to complete action vectors  $Q(s, \mathbf{a})$ , preserving their interdependencies, but avoids exhaustively scoring every action by imposing a tree structure over the space and using a neural network to guide traversal that selectively evaluates a small subset of actions. This results in only a linear number of evaluations per decision, enabling BraVE to scale to high-dimensional combinatorial settings without sacrificing value function fidelity.

#### 3.1 Tree Construction

BraVE imposes a tree structure over the combinatorial action space, assigning a complete  $N$ -dimensional action vector to each node. This vector is constructed by combining the sub-action values explicitly selected along the path from the root with predefined default values (e.g.,  $a_i = 0$  in the binary case) for all unassigned dimensions.

The tree originates from a root node corresponding to the start of traversal, where no sub-actions have been selected. From this root, branches extend to child nodes by explicitly assigning a value  $a_k \in \mathcal{A}_k$  to the  $k$ -th sub-action dimension  $d_k$ . A node at depth  $k$  therefore represents a complete action vector in which the first  $k$  sub-actions ( $a_1, \dots, a_k$ ) have been explicitly set, and the remaining sub-actions ( $a_{k+1}, \dots, a_N$ ) retain their default values. Sibling nodes at depth  $k$  differ from their parent only in the newly assigned component, and differ from each other only in their choice of  $a_k$ . That is, they differ only in the  $k$ -th component of the complete action vector they represent, as illustrated in Figure 1. This dimension-by-dimension construction ensures that reaching a leaf node, where all  $N$  sub-action values have been explicitly assigned, requires traversing at most  $N$  levels.

While this specific  $N$ -depth, dimension-ordered tree is adopted for its computational efficiency, the general BraVE framework places no constraints on the tree structure. Any tree in which each node represents a complete joint action, and in which root-to-leaf paths systematically cover the action space, is a valid instantiation. For example, a flat tree with a single level and  $|\mathcal{A}|$  children — one for each possible joint action — recovers the naive alternative of exhaustively evaluating

$Q(s, \mathbf{a})$  over the entire space. Our implementation, however, deliberately uses the deeper,  $N$ -level structure to guarantee a number of node evaluations linear in  $N$ , which is crucial for tractability in high-dimensional spaces.

This structural flexibility extends beyond tree depth and layout. The ordering of sub-actions, the choice of default values, and the tree topology are all implementation details rather than core components of the method. Regardless of the selected configuration, however, the chosen structure should remain fixed throughout training to ensure consistent semantics for traversal and value estimation. The tree itself may be constructed dynamically at each timestep or precomputed and cached.

BraVE imposes no restrictions on the cardinality of individual sub-actions; each  $a_d$  may be drawn from an arbitrary discrete set  $\mathcal{A}_d$ . For clarity, however, all examples and figures that follow assume a multi-binary action space, where each sub-action is either included ( $a_i = 1$ ) or excluded ( $a_i = 0$ ).

### 3.2 Tree Sparsification

To mitigate overestimation error and stabilize learning, BraVE introduces an inductive bias by **sparsifying the action space tree**, restricting it to include only actions observed in the dataset  $\mathcal{B}$ . This idea is conceptually related to BCQ [15], which constrains policy evaluation to actions deemed plausible by a learned generative model. BraVE, by contrast, enforces this constraint structurally by pruning branches from the tree that correspond to implausible or unsupported sub-action combinations.

This design is particularly effective in real-world settings where certain sub-actions are incompatible and rarely, if ever, appear together. For example, in treatment planning or medication recommendation, specific drug combinations may be avoided due to known adverse interactions. By limiting the tree to feasible actions observed in the data, BraVE avoids evaluating unrealistic behaviors, reduces computational overhead, and curbs value inflation driven by unsupported extrapolation.

### 3.3 Q-Guided Tree Traversal

To compute the greedy action  $\hat{\mathbf{a}}' = \arg \max_{\mathbf{a}'} Q(s', \mathbf{a}'; \theta^-)$  required by Equation (1), BraVE traverses the action space tree using a neural network  $f(\cdot, \cdot; \theta^-)$  to guide decisions at each node. At a node  $\mathbf{a}_{\text{node}}$ , the network receives as input the current state  $s$  and the  $N$ -dimensional action vector corresponding to  $\mathbf{a}_{\text{node}}$ . It outputs a scalar node Q-value  $q = Q(s, \mathbf{a}_{\text{node}}; \theta^-)$  and a vector of *branch values*  $\mathbf{v} \in \mathbb{R}^{M_{\text{children}}^{\max}}$ , where each  $v_j$  estimates the maximum Q-value obtainable in the subtree rooted at the  $j$ -th child. While  $q$  reflects the value of selecting the current node’s complete action, the branch values  $\mathbf{v}$  estimate the best values available in each of the child subtrees.

Though the number of children can vary across nodes, the network output dimensionality remains fixed. Specifically,  $f$  returns one scalar for the current node and  $M_{\text{children}}^{\max} = \max_d |\mathcal{A}_d|$  branch values. For example, if the maximum sub-action cardinality across all dimensions is three, the network produces four outputs total. Following standard practice in structured prediction and reinforcement learning [18, 26] masking is applied to ignore unused entries in  $\mathbf{v}$  for nodes with fewer than  $M_{\text{children}}^{\max}$  children.

Traversal begins at the root node. At each step, the network evaluates  $(q, \mathbf{v})$  at the current node. If  $q \geq \max_j v_j$ , traversal terminates and the corresponding action  $\mathbf{a}_{\text{node}}$  is returned as  $\hat{\mathbf{a}}'$ . Otherwise, the algorithm proceeds to the child indexed by  $\arg \max_j v_j$ . This greedy descent continues until either the termination condition is satisfied or a leaf node is reached. Notably, traversal may terminate at internal nodes rather than always proceeding to a fully specified leaf. This mechanism approximates

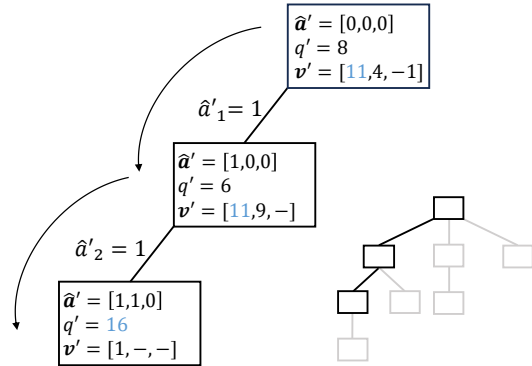


Figure 2: BraVE traversal in a 3-D binary action space (full tree shown bottom-right). Starting from the root  $[0, 0, 0]$ , the agent selects  $\hat{a}'_1 = 1$  since its branch value (11) exceeds both those of alternative children (4,  $-1$ ) and the root’s Q-value (8). Traversal proceeds until reaching  $[1, 1, 0]$ , where the Q-value (16) exceeds the child’s branch value (1); a terminal condition. Masked values ( $-$ ) are ignored.

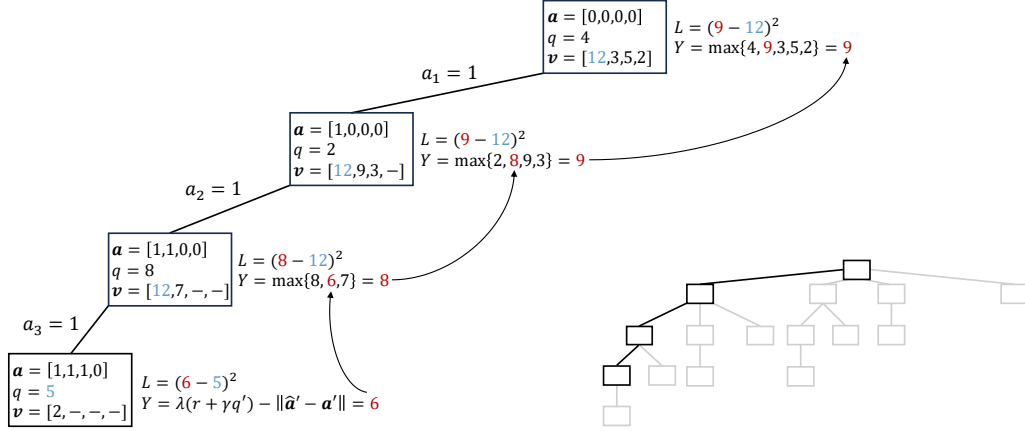


Figure 3: Example of loss propagation in a 4-D binary action space (full tree shown bottom-right). Starting from the node  $[1, 1, 1, 0]$  (bottom left), the target (Equation 5) is propagated to its parent  $[1, 1, 0, 0]$ . The new target is computed as the maximum of the propagated value, the parent’s own Q-value, and the branch values of alternative child nodes. This process recurses up the tree to compute all node losses.

the action with the highest estimated Q-value over the full combinatorial space, while requiring only a linear number of evaluations. A full example of this traversal process is shown in Figure 2.

### 3.4 Loss Computation

BraVE is trained using a behavior-regularized temporal difference (TD) loss that penalizes value estimates for actions unlikely under the dataset. Given a transition  $(s, \mathbf{a}, r, s', \mathbf{a}')$  sampled from the replay buffer  $\mathcal{B}$ , the TD target is computed using the action  $\hat{\mathbf{a}}' = \arg \max_{\mathbf{a}'} Q(s', \mathbf{a}'; \theta^-)$  selected via the tree traversal procedure described in Section 3.3. The loss is defined as:

$$L_{TD}(\theta) = \mathbb{E}_{(s, \mathbf{a}, r, s', \mathbf{a}') \sim \mathcal{B}} \left[ (\lambda (r + \gamma Q(s', \hat{\mathbf{a}}'; \theta^-)) - \|\hat{\mathbf{a}}' - \mathbf{a}'\| - Q(s, \mathbf{a}; \theta))^2 \right], \quad (4)$$

where  $\lambda$  is a regularization coefficient and  $\|\hat{\mathbf{a}}' - \mathbf{a}'\|$  penalizes deviation from the behavior action, following principles introduced in TD3+BC (Equation 2).

We combine this behavior-regularized TD loss with a branch value supervision loss  $L_{\text{BraVE}}$ , resulting in a total objective  $L = \alpha L_{TD} + L_{\text{BraVE}}$ , where  $\alpha$  controls the relative weighting of the TD term. To compute  $L_{\text{BraVE}}$ , we begin from a node  $\mathbf{a}$  sampled from  $\mathcal{B}$  and reuse the TD target

$$Y = \lambda (r + \gamma Q(s', \hat{\mathbf{a}}'; \theta^-)) - \|\hat{\mathbf{a}}' - \mathbf{a}'\| \quad (5)$$

as the supervisory signal. This target is then propagated recursively up the tree. At each step, the target is used to update the parent node’s estimate for the corresponding branch value. The propagated target is updated at each level to reflect the maximum of  $Y$  and the existing sibling branch values, ensuring consistency with the max-based traversal logic. This process continues up to the root, training each node to estimate the highest Q-value accessible through its subtree. The full  $L_{\text{BraVE}}$  computation procedure is provided in Algorithm 1 and illustrated in Figure 3.

### 3.5 Enhancements for Stability and Policy Quality

We mitigate action selection errors due to inaccurate branch value estimates through two complementary mechanisms: a **depth penalty** applied *during training* and **beam search** used *during inference*. During training, we apply a depth-based weighting factor  $\delta$  in the BraVE loss computation. Because the branch value target is propagated upward from a sampled action node to the root, this weighting amplifies the influence of errors closer to the root, where mistakes propagate to more of the tree. At inference time, we use beam search to improve action selection robustness. Instead of committing to a single greedy path, the algorithm retains the top- $W$  actions (ranked by predicted values) at each tree level. The final action is selected from the union of all beams, allowing for broader exploration of high-value combinations and improving policy quality.

## 4 Experimental Evaluation

We evaluate BraVE in the **Combinatorial Navigation Environment (CoNE)**, a high-dimensional discrete control domain designed to stress-test policy learning under large action spaces and sub-action dependencies. In CoNE, actions are formed by selecting subsets of atomic motion primitives (sub-actions), corresponding to directional moves along orthogonal axes. The agent chooses which primitives to activate at each timestep, resulting in a combinatorial action space of size  $|\mathcal{A}| = 2^{2D}$ , where  $D$  is the number of spatial dimensions.

The agent starts from a fixed origin  $s_0$  and must reach a designated goal  $g$ . At each timestep, it receives a negative reward  $r = -\rho(s, g)$  proportional to its Euclidean distance from the goal. Episodes terminate upon reaching the goal (with reward +10) or falling into a pit, a failure state that incurs a penalty of  $r = -10 \cdot \rho(s_0, g)$ . This penalty structure ensures that failure is strictly worse than any successful trajectory, even those that are long or indirect.

CoNE exhibits both combinatorial complexity and tightly coupled action dynamics. Some sub-action combinations are synergistic, such as activating orthogonal directions to move diagonally, opposing movements cancel out, and others lead to failure by directing the agent into hazardous regions of the state space. These structured dependencies mean that the effectiveness of a sub-action often depends critically on the presence or absence of others.

This stands in contrast to discretized variants of popular continuous control environments [28, 31], where sub-actions require coordination but can be learned independently [3]. In CoNE, by contrast, sub-actions that are individually beneficial can be harmful in combination, an effect common in real-world settings such as drug prescription, where treatments may interact antagonistically (see Appendix A).

**Dataset Construction** We generate offline datasets using a stochastic variant of A\*. At each step, the optimal action is selected with probability 0.1, and a random valid action is chosen otherwise. This procedure yields a diverse mixture of trajectories with varying returns, including both near-optimal and suboptimal behavior. The resulting datasets reflect realistic offline settings in which learning must proceed from heterogeneous, partially optimal demonstrations.

**Baselines** We compare BraVE to two representative baselines: (1) Factored Action Spaces (FAS) [3, 27], the state-of-the-art for offline RL in combinatorial action spaces; and (2) Implicit Q-Learning (IQL) [19], a strong general-purpose algorithm included to assess the need for methods purpose-built for combinatorial structures. Following prior work [27], we implement FAS using a factored variant of BCQ [15]. All methods are trained for 20,000 gradient steps and evaluated every 100 steps.

### 4.1 Performance Across Reward Structures and Sub-Action Dependencies

FAS has shown strong performance in offline RL for combinatorial domains [3, 27], however, its effectiveness depends on the assumption that rewards decompose cleanly across sub-actions and that dependencies among sub-actions are weak. These assumptions are often violated in real-world settings, where the effect of one sub-action may depend critically on the value of another. To evaluate

---

#### Algorithm 1 Compute BraVE Loss

---

**Require:**

- $f(\theta)$ : neural network with parameters  $\theta$
  - $f(\theta^-)$ : target network with parameters  $\theta^-$
  - $\{s, \mathbf{a}, r, s', \mathbf{a}'\}$ : transition from  $\mathcal{B}$
  - $\hat{\mathbf{a}}'$ : action selected via tree traversal given  $s$
  - 1:  $(q, \mathbf{v}) \leftarrow f(s, \mathbf{a}; \theta)$
  - 2:  $(q', \mathbf{v}') \leftarrow f(s', \hat{\mathbf{a}}'; \theta^-)$
  - 3:  $Y \leftarrow \lambda(r + \gamma q') - \|\hat{\mathbf{a}}' - \mathbf{a}'\|$
  - 4: **total loss**  $\leftarrow (q - Y)^2$
  - 5: **node**  $\leftarrow \mathbf{a}$
  - 6:  $d \leftarrow 1$
  - 7: **while** node is not *null* **do**
  - 8:     **parent**  $\leftarrow$  GETPARENT(node)
  - 9:      $q, \mathbf{v} \leftarrow f(s, \text{parent}; \theta)$
  - 10:     **children**  $\leftarrow$  GETCHILDREN(parent)
  - 11:      $i \leftarrow$  index of node in children
  - 12:     **loss**  $\leftarrow ((\mathbf{v}[i] - Y) * \delta d)^2$
  - 13:     **total loss**  $\leftarrow$  total loss + loss
  - 14:      $\mathbf{v}[i] \leftarrow Y$
  - 15:      $Y \leftarrow \max(q, \mathbf{v})$
  - 16:     **node**  $\leftarrow$  parent
  - 17:      $d \leftarrow d + 1$
  - 18: **end while**
  - 19: **return** total loss/ $d$
-

| $ \mathcal{A} $ | BraVE           | FAS              | IQL              |
|-----------------|-----------------|------------------|------------------|
| 16              | 1.5 $\pm$ 0.0   | 1.5 $\pm$ 0.0    | -0.4 $\pm$ 1.5   |
| 64              | -0.4 $\pm$ 0.0  | -0.4 $\pm$ 0.0   | -6.1 $\pm$ 3.2   |
| 256             | -2.0 $\pm$ 0.1  | -2.3 $\pm$ 0.6   | -9.8 $\pm$ 4.5   |
| 1024            | -3.4 $\pm$ 0.1  | -10.8 $\pm$ 2.3  | -13.1 $\pm$ 5.8  |
| 4096            | -6.9 $\pm$ 1.6  | -7.3 $\pm$ 3.1   | -13.5 $\pm$ 5.7  |
| $\sim$ 16k      | -6.1 $\pm$ 0.4  | -25.6 $\pm$ 33.3 | -15.4 $\pm$ 6.0  |
| $\sim$ 65k      | -8.2 $\pm$ 2.2  | -24.4 $\pm$ 10.4 | -27.0 $\pm$ 11.5 |
| $\sim$ 260k     | -13.8 $\pm$ 5.4 | -42.2 $\pm$ 32.3 | -48.4 $\pm$ 17.7 |
| $\sim$ 1M       | -9.6 $\pm$ 1.2  | -21.4 $\pm$ 18.2 | -53.7 $\pm$ 31.0 |
| $\sim$ 4M       | -18.6 $\pm$ 8.3 | -33.9 $\pm$ 27.0 | -66.9 $\pm$ 31.6 |

Table 1: In environments with non-factorizable reward structures and no sub-action dependencies BraVE and FAS perform similarly in low-dimensional settings, but as action dimensionality increases, BraVE maintains high returns and stable policies, while FAS’s performance deteriorates. IQL performs worst in all settings.

BraVE in precisely these challenging conditions, we construct a suite of CoNE environments that systematically vary along both axes of complexity.

We measure performance across 10 randomly generated environments in each of two settings: the first includes non-factorizable reward structures without sub-action dependencies, and the second includes both non-factorizable rewards and interdependent sub-actions. For each task, we vary dimensionality from 2-D ( $|\mathcal{A}| = 16$ ) to 11-D ( $|\mathcal{A}| > 4$  million), where each additional dimension introduces two new sub-actions. Each environment has size 5 in every dimension. The agent starts in the top-left corner and must reach a goal in the bottom-right. Results are averaged over five random seeds.

**Non-Factorizable Reward Structures Only** We begin with environments that contain no pits. In these settings, the transition dynamics are factorizable across sub-actions. However, the reward function cannot be linearly decomposed. As shown in Table 1, FAS performs comparably to BraVE in low-dimensional tasks. As dimensionality increases, however, the modeling bias introduced by FAS’s linear decomposition causes the learned Q-values to diverge from the true values, degrading its performance. BraVE, by contrast, remains stable across all action space sizes, as it evaluates complete actions rather than marginal components. IQL performs significantly worse than both BraVE and FAS across all action space sizes, suggesting that methods not explicitly designed for combinatorial actions struggle even when transitions are factorizable. Complete learning curves are provided in Appendix B.1.

| Pit % | BraVE            | FAS                | IQL               |
|-------|------------------|--------------------|-------------------|
| 0     | -8.2 $\pm$ 2.2   | -24.4 $\pm$ 10.4   | -27.0 $\pm$ 11.5  |
| 5     | -19.0 $\pm$ 2.3  | -78.4 $\pm$ 99.7   | -85.8 $\pm$ 45.0  |
| 10    | -16.9 $\pm$ 3.3  | -140.4 $\pm$ 177.1 | -88.1 $\pm$ 50.1  |
| 25    | -42.9 $\pm$ 43.3 | -178.6 $\pm$ 212.8 | -82.8 $\pm$ 52.0  |
| 50    | -54.8 $\pm$ 47.9 | -902.6 $\pm$ 274.1 | -106.4 $\pm$ 42.8 |
| 75    | -42.9 $\pm$ 34.3 | -942.8 $\pm$ 278.1 | -110.0 $\pm$ 34.3 |
| 100   | -41.6 $\pm$ 22.4 | -1131.4 $\pm$ 0.0  | -112.4 $\pm$ 22.8 |

Table 2: BraVE maintains stable performance across environments with non-factorizable rewards and sub-action dependencies, whereas FAS exhibits a sharp decline when pits occupy at least half of the interior states. IQL performance also degrades as sub-action dependencies increase.

**Non-Factorizable Rewards and Sub-Action Dependencies** We next evaluate performance under increasing sub-action dependency induced by hazardous transitions. In an 8-D environment ( $|\mathcal{A}| = 65, 536$ ), we vary the number of pits from 5% to 100% of the 6,561 interior (non-boundary) states, ensuring that there is always a feasible path to the goal along the boundary of the state space. As

| $ \mathcal{S} $ | BraVE           | FAS                | IQL              |
|-----------------|-----------------|--------------------|------------------|
| 25              | $-7.5 \pm 2.4$  | $-531.5 \pm 31.4$  | $-12.1 \pm 5.8$  |
| 125             | $-2.9 \pm 0.2$  | $-579.8 \pm 7.2$   | $-14.1 \pm 13.6$ |
| 625             | $-5.6 \pm 1.5$  | $-480.3 \pm 152.9$ | $-22.4 \pm 20.6$ |
| 3125            | $-6.3 \pm 0.7$  | $-147.4 \pm 292.6$ | $-28.0 \pm 22.8$ |
| 15625           | $-12.4 \pm 7.9$ | $-18.9 \pm 4.6$    | $-37.8 \pm 17.4$ |

Table 3: When sub-action dependencies are sparse but critical, BraVE performs reliably even in small state spaces with high-risk actions. FAS approaches BraVE’s performance only once the joint action space exceeds 15 thousand. IQL performs worse than BraVE in all settings.

shown in Table 2, BraVE maintains stable performance across all pit densities. FAS, by contrast, degrades sharply once pits occupy half of the interior, and IQL declines steadily as dependency strength increases. These results highlight BraVE’s ability to handle tightly coupled decision-making, even when adverse interactions between sub-actions are common. Complete learning curves are provided in Appendix B.2.

**Sparse but Critical Sub-Action Dependencies** Having established that BraVE performs well under strong sub-action coupling, we examine settings with only five pits, representing a negligible fraction of the state space in high dimensions. We continue scaling the state space until BraVE and FAS converge to similar average returns, allowing us to assess how each method handles **sparse but critical dependencies**. As shown in Table 3, BraVE performs reliably even when the state space is small and each action carries substantial risk. FAS, by contrast, requires a much larger state space before the influence of the pits becomes diluted and its performance approaches that of BraVE. This demonstrates that even a small number of pits is sufficient to invalidate naive factorizations. Complete learning curves are provided in Appendix B.3.

## 4.2 Online Fine-Tuning

BraVE’s data-driven tree sparsification (Section 3.2) inherently constrains action selection to observed behaviors, a principle shared by offline methods that model the behavior policy using generative approaches [15]. However, BraVE imposes this constraint structurally, eliminating the reliance on an explicit behavior model that can complicate online fine-tuning [23]. Consequently, BraVE can be directly fine-tuned online without modification. Appendix C shows that BraVE matches IQL’s performance during fine-tuning when both methods begin from comparable offline initialization.

## 4.3 Ablations and Hyperparameters

We conduct ablation studies to assess the impact of important design choices in BraVE. We first examine the depth penalty parameter  $\delta$ , which scales the contribution of branch value errors based on a node’s depth, assigning greater weight to updates near the root where misestimates affect larger portions of the tree. Next, we vary the loss weight  $\alpha$  to study the trade-off between the behavior-regularized TD loss and the BraVE loss. To isolate the effect of BraVE’s tree structure and Q-guided traversal, we compare against a DQN-based variant trained using BraVE’s loss (Equation 4) but without tree-based action selection or branch value propagation. Finally, we evaluate how the beam width used during inference affects both policy quality and computational cost. Full results are provided in Appendix D.

# 5 Related Work

## 5.1 Tree-based RL

Tree-based methods in RL have historically been applied to ordered decision processes. Most notably, Monte Carlo Tree Search (MCTS) [6], as used in AlphaZero [26], recursively selects actions using the PUCT algorithm [2]. However, its sequential structure makes it ill-suited for unordered action spaces like those considered here, where sub-actions must be selected simultaneously.

TreeQN [10] blends model-free RL with online planning by constructing a tree over learned state representations, refining value estimates via tree backups. Differentiable decision trees (DDTs) [25] enable gradient-based learning in RL by replacing the hard splits typical of decision trees with smooth transitions, which can later be discretized for interpretability. In the offline setting, Ernst et al. [9] apply tree-based regression (e.g., CART, Kd-trees) to approximate Q-functions via fitted Q-iteration.

## 5.2 Combinatorial Action Spaces

Many RL approaches have been developed for combinatorial action spaces, particularly in domain-specific contexts such as text-based games [16, 17, 34], routing [7, 24], TSP [4], and resource allocation [5]. These methods often depend on domain structure, whereas BraVE is domain-agnostic.

General-purpose approaches include distributed action representations [29], curriculum-based action space growth [11], and search-based amortized Q-learning [32], which replaces exact action maximization with optimization over sampled proposals. Wol-DDPG [8] embeds discrete actions into continuous spaces, though this approach has been found to be ineffective in unordered settings [5]. Notably, these are online approaches, and their application to offline settings is often non-trivial. For example, Zhao et al. [35] rely on state-action visitation counts, which are generally infeasible to obtain offline.

Closer to our setting, Tang et al. [27] and Beeson et al. [3] evaluate Factored Action Spaces (FAS in our experiments), which linearly decompose the Q-function by conditioning each term on a single sub-action. While this reduces dimensional complexity, it relies on sub-action independence; a condition that often fails in real-world domains. Crucially, these limitations are algorithm-agnostic and apply to factorized variants of all offline RL methods. BraVE, by contrast, structures the action space to retain sub-action dependencies without incurring exponential cost.

## 6 Discussion and Conclusion

In many real-world decision-making problems, combinatorial action spaces arise from the simultaneous selection of multiple sub-actions. Offline RL in these settings remains challenging due to the cost of optimization and the difficulty of modeling sub-action dependencies from fixed datasets. Standard methods do not scale, while factorized approaches improve tractability at the expense of expressivity. We present **Branch Value Estimation (BraVE)**, an offline RL method for discrete combinatorial action spaces. By structuring the action space as a tree, BraVE captures sub-action dependencies while reducing the number of actions evaluated per timestep, enabling scalability to large spaces. BraVE outperforms state-of-the-art baselines across environments with varying action space sizes and sub-action dependencies.

While BraVE demonstrates strong performance, several limitations and opportunities for future work remain. First, the current implementation relies on a fixed, predefined ordering of sub-action dimensions for tree construction. This ordering can influence performance, particularly when sub-action dependencies do not align with the chosen sequence. Future work could explore methods for learning or adapting this ordering. Second, although BraVE scales with the number of sub-action dimensions ( $N$ ), its efficiency may degrade when individual sub-action dimensions ( $|\mathcal{A}_d|$ ) have extremely high cardinality, as this increases the branching factor and the size of the output layer for branch values. Third, computing  $L_{BraVE}$  involves backpropagating through multiple parent node evaluations per sampled action. While necessary for consistent value estimation, this adds overhead compared to standard Q-learning updates, especially in deep trees. Inference, however, remains efficient due to linear-time traversal. Next, like all offline RL methods, BraVE’s performance depends on the quality and coverage of the offline dataset. Although tree sparsification leverages available data effectively, generalizing to unseen action combinations not represented in the sparsified tree remains a challenge. Finally, our empirical validation on the CoNE benchmark, while designed to test key capabilities, could be extended to a broader range of combinatorial tasks to further assess generalizability.

Despite these limitations, BraVE provides a flexible and extensible foundation for future research on combinatorial action spaces. We believe its applicability extends well beyond the specific setting explored in this paper. In particular, constrained RL presents a promising direction, as BraVE’s tree structure naturally supports the exclusion of inadmissible action combinations through pruning.

## References

- [1] Rishabh Agarwal, Dale Schuurmans, and Mohammad Norouzi. An optimistic perspective on offline reinforcement learning. In *International conference on machine learning*, pages 104–114. PMLR, 2020.
- [2] David Auger, Adrien Couetoux, and Olivier Teytaud. Continuous upper confidence trees with polynomial exploration–consistency. In *Machine Learning and Knowledge Discovery in Databases: European Conference, ECML PKDD 2013, Prague, Czech Republic, September 23-27, 2013, Proceedings, Part I 13*, pages 194–209. Springer, 2013.
- [3] Alex Beeson, David Ireland, and Giovanni Montana. An investigation of offline reinforcement learning in factorisable action spaces. *arXiv preprint arXiv:2411.11088*, 2024.
- [4] Irwan Bello, Hieu Pham, Quoc V Le, Mohammad Norouzi, and Samy Bengio. Neural combinatorial optimization with reinforcement learning. *arXiv preprint arXiv:1611.09940*, 2016.
- [5] Changyu Chen, Ramesha Karunasena, Thanh Nguyen, Arunesh Sinha, and Pradeep Varakantham. Generative modelling of stochastic actions with arbitrary constraints in reinforcement learning. *Advances in Neural Information Processing Systems*, 36, 2024.
- [6] Rémi Coulom. Efficient selectivity and backup operators in monte-carlo tree search. In *International conference on computers and games*, pages 72–83. Springer, 2006.
- [7] Arthur Delarue, Ross Anderson, and Christian Tjandraatmadja. Reinforcement learning with combinatorial actions: An application to vehicle routing. *Advances in Neural Information Processing Systems*, 33:609–620, 2020.
- [8] Gabriel Dulac-Arnold, Richard Evans, Hado van Hasselt, Peter Sunehag, Timothy Lillicrap, Jonathan Hunt, Timothy Mann, Theophane Weber, Thomas Degris, and Ben Coppin. Deep reinforcement learning in large discrete action spaces. *arXiv preprint arXiv:1512.07679*, 2015.
- [9] Damien Ernst, Pierre Geurts, and Louis Wehenkel. Tree-based batch mode reinforcement learning. *Journal of Machine Learning Research*, 6, 2005.
- [10] Gregory Farquhar, Tim Rocktäschel, Maximilian Igl, and Shimon Whiteson. Treeqn and atrec: Differentiable tree-structured models for deep reinforcement learning. *arXiv preprint arXiv:1710.11417*, 2017.
- [11] Gregory Farquhar, Laura Gustafson, Zeming Lin, Shimon Whiteson, Nicolas Usunier, and Gabriel Synnaeve. Growing action spaces. In *International Conference on Machine Learning*, pages 3040–3051. PMLR, 2020.
- [12] Yuwei Fu, Wu Di, and Benoit Boulet. Batch reinforcement learning in the real world: A survey. In *Offline RL Workshop, NeuroIPS*, 2020.
- [13] Scott Fujimoto and Shixiang Shane Gu. A minimalist approach to offline reinforcement learning. *Advances in neural information processing systems*, 34:20132–20145, 2021.
- [14] Scott Fujimoto, Herke Hoof, and David Meger. Addressing function approximation error in actor-critic methods. In *International conference on machine learning*, pages 1587–1596. PMLR, 2018.
- [15] Scott Fujimoto, David Meger, and Doina Precup. Off-policy deep reinforcement learning without exploration. In *International conference on machine learning*, pages 2052–2062. PMLR, 2019.
- [16] Ji He, Jianshu Chen, Xiaodong He, Jianfeng Gao, Lihong Li, Li Deng, and Mari Ostendorf. Deep reinforcement learning with a natural language action space. *arXiv preprint arXiv:1511.04636*, 2015.
- [17] Ji He, Mari Ostendorf, Xiaodong He, Jianshu Chen, Jianfeng Gao, Lihong Li, and Li Deng. Deep reinforcement learning with a combinatorial action space for predicting popular reddit threads. *arXiv preprint arXiv:1606.03667*, 2016.

- [18] Shengyi Huang and Santiago Ontañón. A closer look at invalid action masking in policy gradient algorithms. *arXiv preprint arXiv:2006.14171*, 2020.
- [19] Ilya Kostrikov, Ashvin Nair, and Sergey Levine. Offline reinforcement learning with implicit q-learning. *arXiv preprint arXiv:2110.06169*, 2021.
- [20] Aviral Kumar, Aurick Zhou, George Tucker, and Sergey Levine. Conservative q-learning for offline reinforcement learning. *Advances in neural information processing systems*, 33: 1179–1191, 2020.
- [21] Sascha Lange, Thomas Gabel, and Martin Riedmiller. Batch reinforcement learning. In *Reinforcement learning: State-of-the-art*, pages 45–73. Springer, 2012.
- [22] Sergey Levine, Aviral Kumar, George Tucker, and Justin Fu. Offline reinforcement learning: Tutorial, review, and perspectives on open problems. *arXiv preprint arXiv:2005.01643*, 2020.
- [23] Ashvin Nair, Abhishek Gupta, Murtaza Dalal, and Sergey Levine. Awac: Accelerating online reinforcement learning with offline datasets. *arXiv preprint arXiv:2006.09359*, 2020.
- [24] Mohammadreza Nazari, Afshin Oroojlooy, Lawrence Snyder, and Martin Takác. Reinforcement learning for solving the vehicle routing problem. *Advances in neural information processing systems*, 31, 2018.
- [25] Andrew Silva, Matthew Gombolay, Taylor Killian, Ivan Jimenez, and Sung-Hyun Son. Optimization methods for interpretable differentiable decision trees applied to reinforcement learning. In *International conference on artificial intelligence and statistics*, pages 1855–1865. PMLR, 2020.
- [26] David Silver, Thomas Hubert, Julian Schrittwieser, Ioannis Antonoglou, Matthew Lai, Arthur Guez, Marc Lanctot, Laurent Sifre, Dhharshan Kumaran, Thore Graepel, et al. A general reinforcement learning algorithm that masters chess, shogi, and go through self-play. *Science*, 362(6419):1140–1144, 2018.
- [27] Shengpu Tang, Maggie Makar, Michael Sjoding, Finale Doshi-Velez, and Jenna Wiens. Leveraging factored action spaces for efficient offline reinforcement learning in healthcare. *Advances in Neural Information Processing Systems*, 35:34272–34286, 2022.
- [28] Yuval Tassa, Yotam Doron, Alistair Muldal, Tom Erez, Yazhe Li, Diego de Las Casas, David Budden, Abbas Abdolmaleki, Josh Merel, Andrew Lefrancq, et al. Deepmind control suite. *arXiv preprint arXiv:1801.00690*, 2018.
- [29] Arash Tavakoli, Fabio Pardo, and Petar Kormushev. Action branching architectures for deep reinforcement learning. In *Proceedings of the aaai conference on artificial intelligence*, volume 32, 2018.
- [30] Sebastian Thrun and Anton Schwartz. Issues in using function approximation for reinforcement learning. In *Proceedings of the 1993 connectionist models summer school*, 1993.
- [31] Mark Towers, Ariel Kwiatkowski, Jordan Terry, John U. Balis, Gianluca De Cola, Tristan Deleu, Manuel Goulão, Andreas Kallinteris, Markus Krimmel, Arjun KG, Rodrigo Perez-Vicente, Andrea Pierré, Sander Schulhoff, Jun Jet Tai, Hannah Tan, and Omar G. Younis. Gymnasium: A standard interface for reinforcement learning environments, 2024. URL <https://arxiv.org/abs/2407.17032>.
- [32] Tom Van de Wiele, David Warde-Farley, Andriy Mnih, and Volodymyr Mnih. Q-learning in enormous action spaces via amortized approximate maximization. *arXiv preprint arXiv:2001.08116*, 2020.
- [33] Jinsung Yoon, James Jordon, and Mihaela Schaar. Asac: Active sensing using actor-critic models. In *Machine Learning for Healthcare Conference*, pages 451–473. PMLR, 2019.
- [34] Tom Zahavy, Matan Haroush, Nadav Merlis, Daniel J Mankowitz, and Shie Mannor. Learn what not to learn: Action elimination with deep reinforcement learning. *Advances in neural information processing systems*, 31, 2018.

- [35] Xutong Zhao, Yangchen Pan, Chenjun Xiao, Sarath Chandar, and Janarthanan Rajendran. Conditionally optimistic exploration for cooperative deep multi-agent reinforcement learning. In *Uncertainty in Artificial Intelligence*, pages 2529–2540. PMLR, 2023.

## A Limitations of Standard Value-Based Estimation and Q-Function Factorization in Combinatorial Action Spaces with Sub-Action Dependencies

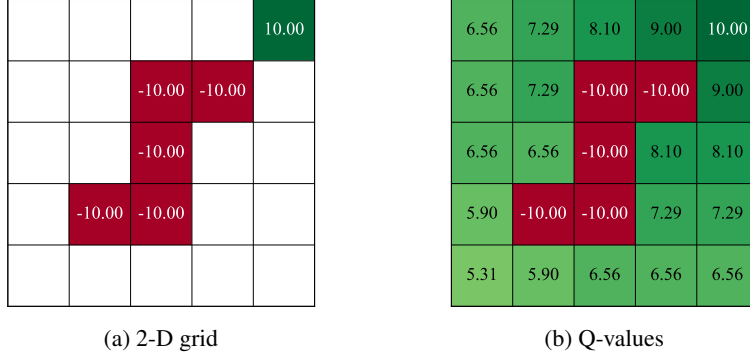


Figure 4: A 2-D grid with five pits and the true maximum Q-values in each state.

Consider a two-dimensional grid with five pits, which provides a simplified instance of CoNE, allowing us to clearly illustrate the limitations of standard methods. At each state, the agent chooses from 16 possible actions ( $|\mathcal{A}| = 16$ ), corresponding to combinations of movement directions (e.g.,  $\emptyset$ , [U], [UD], [UDL], [ULR], [UDLR], [D], [DR],  $\dots$ ). Transitions yield a reward of  $r = 0$  unless they lead to the goal ( $r = 10$ ) or a pit ( $r = -10$ ), as shown in Figure 4a.

Sub-action dependencies are inherently captured by the standard Q-function, as they affect both immediate rewards and future returns:

$$Q_\pi(s, a) = r(s, a) + \gamma \sum_{s' \in \mathcal{S}} p(s, a, s') \left( \sum_{a' \in \mathcal{A}} \pi(a' | s') Q_\pi(s', a') \right).$$

Thus, the agent can learn the true maximum Q-value in each state (Figure 4b) and, consequently, recover the optimal policy.

Accurately estimating the Q-function is challenging in combinatorial action spaces, where the number of possible actions grows exponentially with the action dimension. This complexity limits the applicability of value-based RL methods, such as IQL, which require estimating values for all actions.

More specifically, IQL’s policy loss is defined as:

$$L_\pi(\phi) = \mathbb{E}_{(s,a) \sim \mathcal{B}} \left[ \exp(\beta (Q(s, a; \theta^-) - V(s; \psi))) \log \pi_\phi(a | s) \right].$$

In discrete action settings, the policy  $\pi_\phi(a | s)$  is typically parameterized as a flat categorical distribution. That is, a policy network maps the state  $s$  to a vector of logits  $\ell_\phi(s) \in \mathbb{R}^{|\mathcal{A}|}$ , where  $|\mathcal{A}|$  is the number of discrete actions. The softmax function then transforms these logits into a probability distribution:

$$\pi_\phi(a | s) = \frac{\exp(\ell_\phi(s)_a)}{\sum_{b=1}^{|\mathcal{A}|} \exp(\ell_\phi(s)_b)}.$$

This formulation requires a forward pass through the policy network to produce logits for all possible actions, incurring computational cost and modeling complexity that scale with  $|\mathcal{A}|$ .

BraVE evaluates only a subset of possible actions at each timestep, allowing it to exploit the Q-function’s capacity to capture sub-action dependencies without predicting an exponential number of action values or logits simultaneously. Factored approaches (FAS) [3, 27], by contrast, simplify computation by linearly decomposing the Q-function, conditioning each component on a single sub-action and the full state. While this reduces the dimensional complexity of the action space, it imposes structural constraints on the reward and Q-function definitions:

$$r(s, a) = \sum_{d=1}^D r_d(s, a_d) \quad \text{and} \quad Q(s, a) = \sum_{d=1}^D q_d(s, a_d), \quad (6)$$

that may limit expressiveness in settings with sub-action dependencies and cause the Q-function to *diverge*.

More specifically, when sub-actions are combined (e.g., “up” + “left”), FAS retrieves partial Q-values  $q_1(s, \text{up})$  and  $q_2(s, \text{left})$  from different next states, rather than from a single consistent next state determined by the combined action. This results in artificially inflated values, as the summations in Equation (6) incorrectly assume independence. Iterative Bellman updates, as used in Q-learning, amplify this inconsistency, ultimately causing Q-value divergence.

The independence assumption holds in discretized variants of popular continuous control environments, where sub-actions typically influence distinct parts of the state space [28, 31]. However, this assumption is violated in many real-world settings, a limitation explicitly acknowledged in the FAS literature [3, 27].

## B CoNE Learning Curves

We compare BraVE’s performance to two state-of-the-art baselines: Factored Action Spaces (FAS) [27, 3], which learns linearly decomposable Q-functions for offline combinatorial action spaces, and Implicit Q-Learning (IQL) [19], a general-purpose offline RL method. All methods are evaluated across 20 instances of CoNE. In CoNE, the sizes of both the action and state spaces increase exponentially with the environment’s dimensionality: a  $D$ -dimensional setting with  $M$  positions per axis yields  $|\mathcal{A}| = 2^{2D}$  joint actions and  $|\mathcal{S}| = M^D$  distinct states. All experiments were conducted on a single NVIDIA A40 GPU using Python 3.9 and PyTorch 2.6.

In all curves, results are averaged over 5 seeds; shaded regions indicate one standard deviation.

### B.1 Non-Factorizable Reward Structures Only

In environments without pits, transition dynamics are factorizable across sub-actions. The reward function, however, remains non-linear and cannot be decomposed. Below we present the training curves corresponding to the results in Table 1.

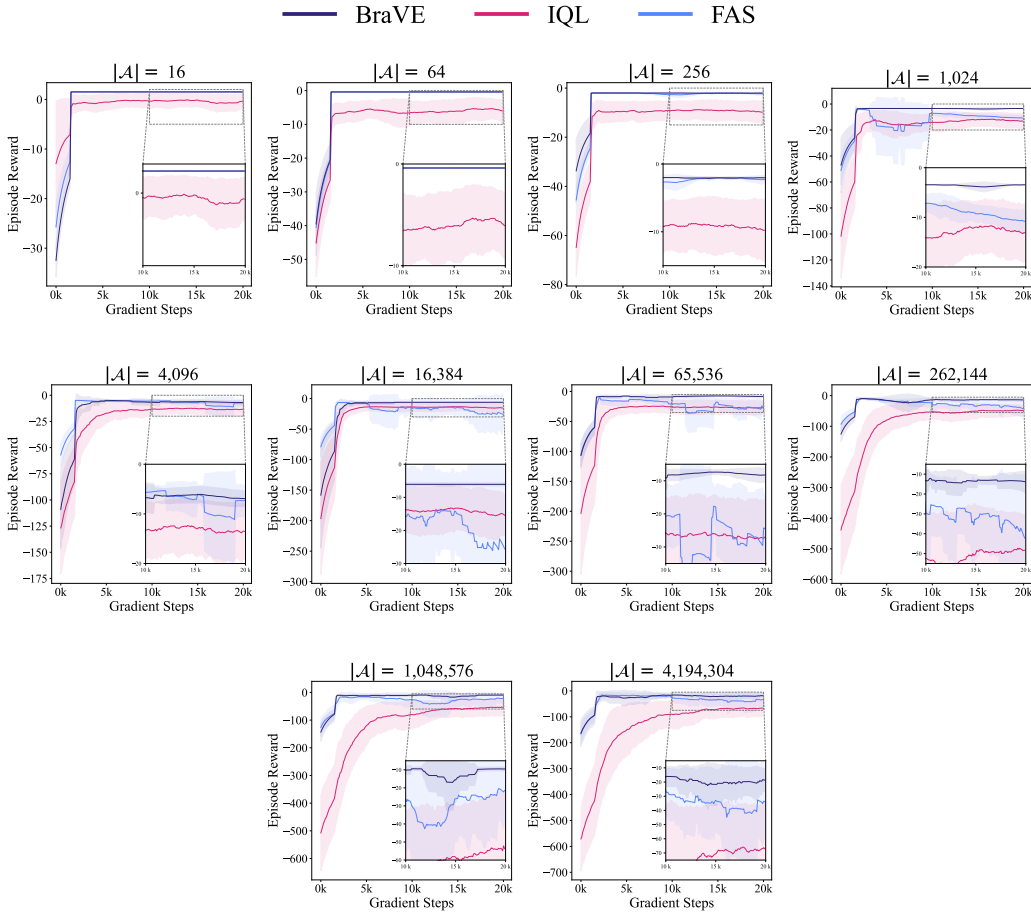


Figure 5: Learning curves for BraVE, FAS, and IQL in environments with non-factorizable reward structures but no sub-action dependencies.

In low-dimensional settings, FAS performs similarly to BraVE, but its performance degrades as dimensionality increases due to the bias introduced by linear Q-function decomposition. BraVE, by contrast, remains stable across all action space sizes by evaluating joint actions directly. IQL performs relatively poorly in all configurations, indicating that general-purpose offline RL methods struggle even when transition dynamics are factorizable.

## B.2 Non-Factorizable Reward Structures and Sub-Action Dependencies

To assess performance under increasing sub-action dependencies, we introduce hazardous transitions by varying the density of pits in an 8-D environment ( $|\mathcal{A}| = 65,536$ ). The number of pits ranges from 5% to 100% of the 6,561 interior (non-boundary) states. Below we present the training curves corresponding to the results in Table 2.

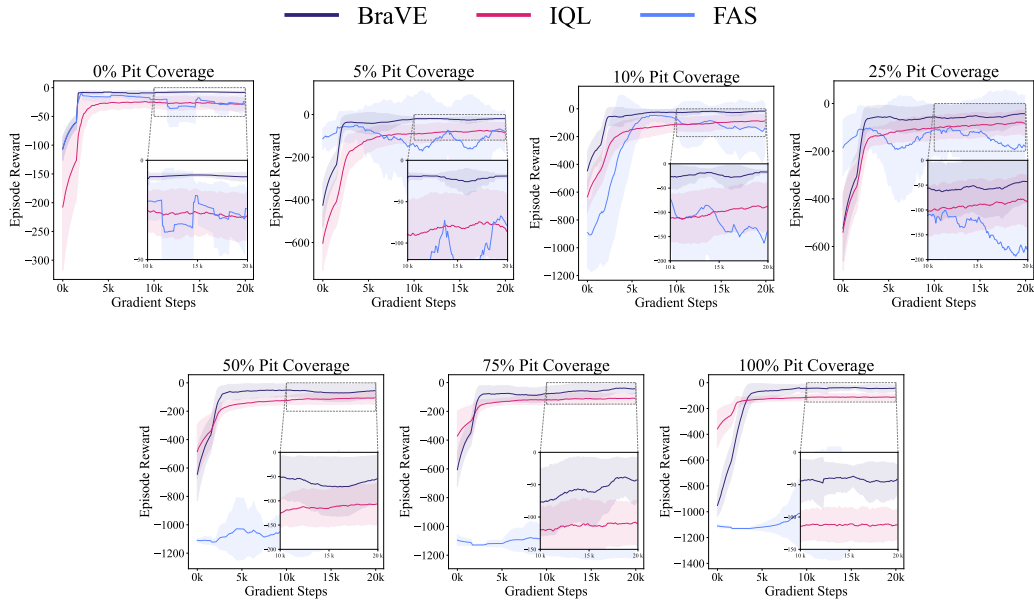


Figure 6: Learning curves for BraVE, FAS, and IQL in environments with non-factorizable reward structures and sub-action dependencies.

BraVE maintains stable returns across all pit densities, whereas FAS degrades sharply when pits cover at least half the interior states. IQL performance degrades as dependency strength increases. These results demonstrate BraVE’s effectiveness in environments with tightly coupled sub-action effects and frequent adverse interactions.

### B.3 Sparse but Critical Sub-Action Dependencies

To isolate the effect of sparse but critical sub-action dependencies, we consider environments with only five pits, representing a negligible fraction of the state space in higher dimensions. Starting in the 2-D environment, we progressively scale the state space until BraVE and FAS converge to similar average returns, allowing us to evaluate how each method handles **low-frequency but high-impact hazards**. Below we present the training curves corresponding to the results in Table 3.

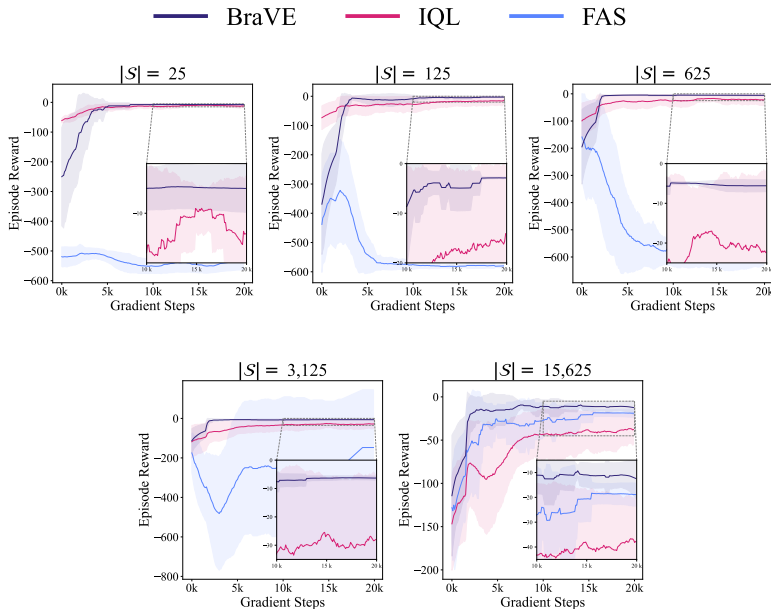


Figure 7: Learning curves for BraVE, FAS, and IQL in environments with sparse but critical sub-action dependencies.

BraVE performs reliably across all settings with sparse but critical sub-action dependencies even when the environment is small and each action carries significant risk. FAS, by contrast, requires much larger state spaces before the influence of the pits diminishes and its performance approaches that of BraVE. These findings indicate that even a small number of hazardous transitions can invalidate simplistic factorizations. IQL performs worse than BraVE in all settings.

## C Online Fine-Tuning After Offline Learning

To evaluate BraVE’s capacity for online fine-tuning, we compare it to IQL, a method known for strong online adaptation following offline pretraining. FAS is excluded from this experiment because, as a factorized version of BCQ, it is not suited to online fine-tuning [23].

We conduct this experiment in an 8-D environment with 3,281 pits (50% of interior states), which is empirically the most challenging 8-D CoNE configuration for BraVE. Success in this setting best indicates generalizability to environments where BraVE demonstrates stronger performance.

Both methods are first trained offline for 1,500 gradient steps, after which BraVE achieves an average return of -226.1 compared to IQL’s -259.4. We terminate offline training at this point, as BraVE consistently surpasses IQL beyond this threshold (see Figure 6). Online fine-tuning then proceeds for an additional 5,000 environment steps.

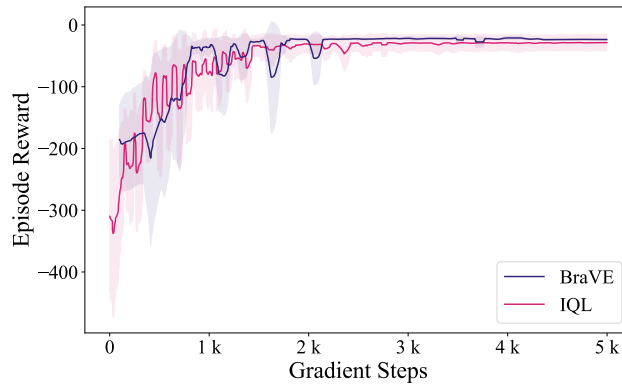


Figure 8: Learning curves for finetuning BraVE and IQL after 1,500 offline gradient steps.

As shown in Figure 8, the methods achieve comparable final performance during fine-tuning, with BraVE slightly outperforming IQL.

## D Ablation and Hyperparameter Learning Curves

This section presents learning curves from four ablation and hyperparameter studies: (1) the effect of varying the depth penalty  $\delta$ , (2) BraVE’s sensitivity to  $\alpha$ , the weight of the TD error in the total loss, (3) the importance of BraVE’s tree structure, and (4) the effect of beam width on both return and computational overhead. A summary of these results appears in Figure 9, with full details provided in Appendices D.1, D.2, D.3, and D.4, respectively. All experiments are conducted in five-pit environments.

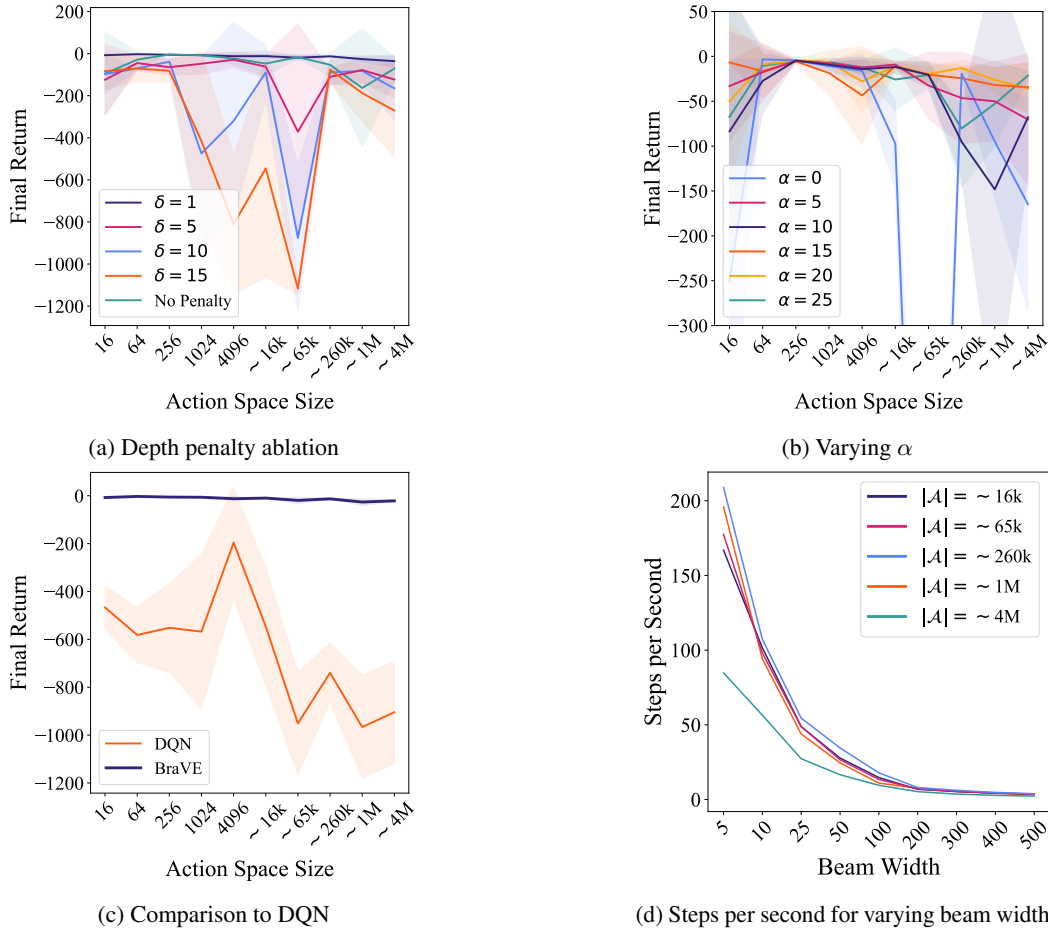


Figure 9: A small depth penalty ( $\delta = 1$ ) yields the best performance across all environments (Figure 9a). Performance remains relatively stable across a range of  $\alpha$  values; however, omitting the TD loss entirely ( $\alpha = 0$ ) can result in suboptimal policies (Figure 9b). Although constraining the DQN to select actions within  $\mathcal{B}$  introduces an inductive bias, it fails to produce a viable policy (Figure 9c). Beam width has minimal practical impact on runtime as inference remains under one second even with beam widths well above the optimal setting (Figure 9d).

## D.1 Depth Penalty Ablation

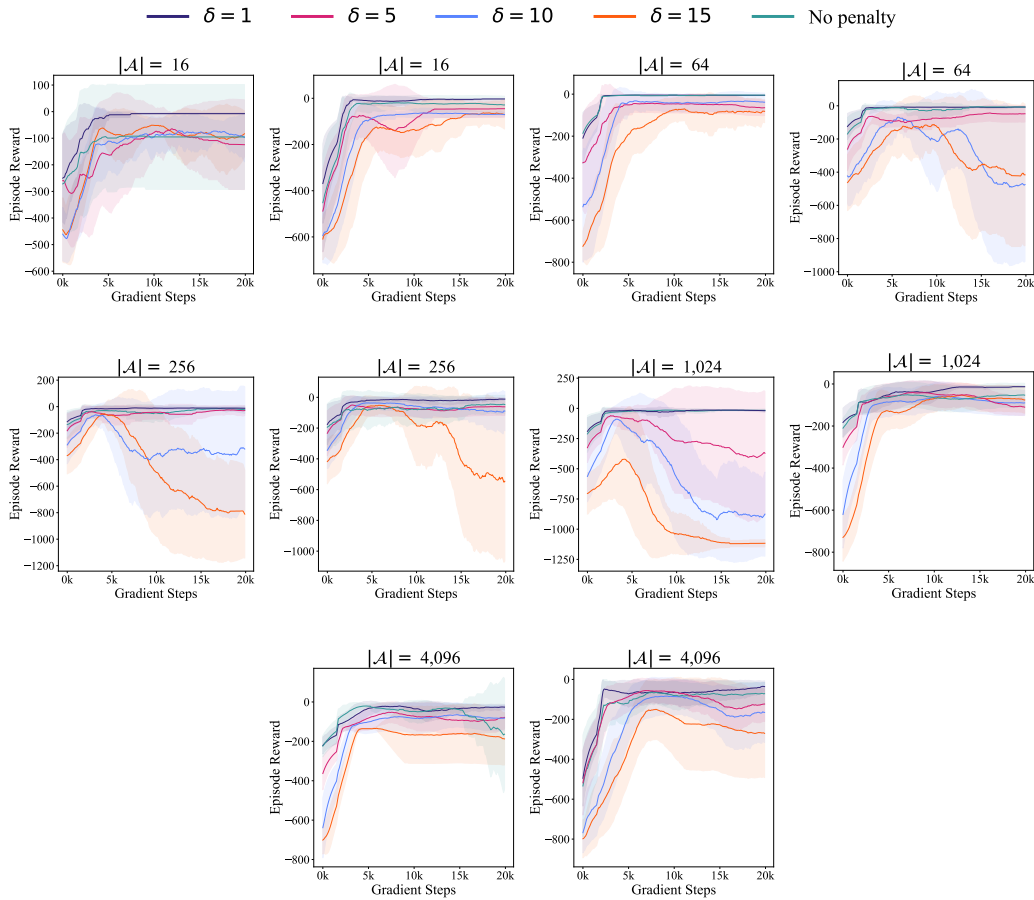


Figure 10: Learning curves for BraVE with varying depth penalty values ( $\delta$ ).

While the depth penalty improves performance, it should remain small;  $\delta = 1$  yields optimal results across nearly all environments.

## D.2 Varying TD Weight in Loss

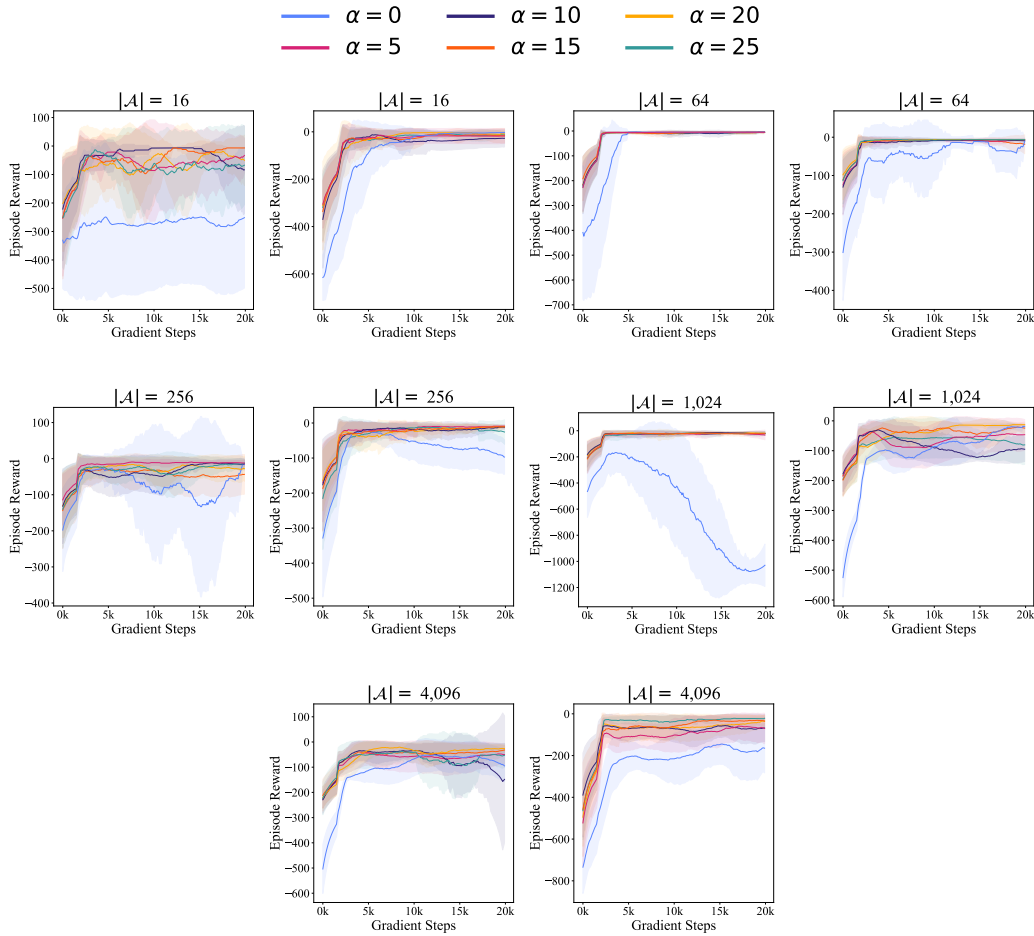


Figure 11: Learning curves for BraVE with varying TD loss weight values ( $\alpha$ ).

Performance is relatively stable across  $\alpha$  values in low-dimensional environments, with the exception of the 2-D case, where the high pit density makes accurate decision-making critical. In higher-dimensional settings, BraVE becomes more sensitive to the choice of  $\alpha$ . In particular, omitting the TD loss term ( $\alpha = 0$ ) can result in catastrophic failures, especially in complex environments such as the 8-D setting.

### D.3 Comparison to DQN

To isolate the effect of BraVE’s tree structure, we compare it to a DQN constrained to selecting actions from the dataset  $\mathcal{B}$  and trained using BraVE’s behavior-regularized TD loss (Equation 4).

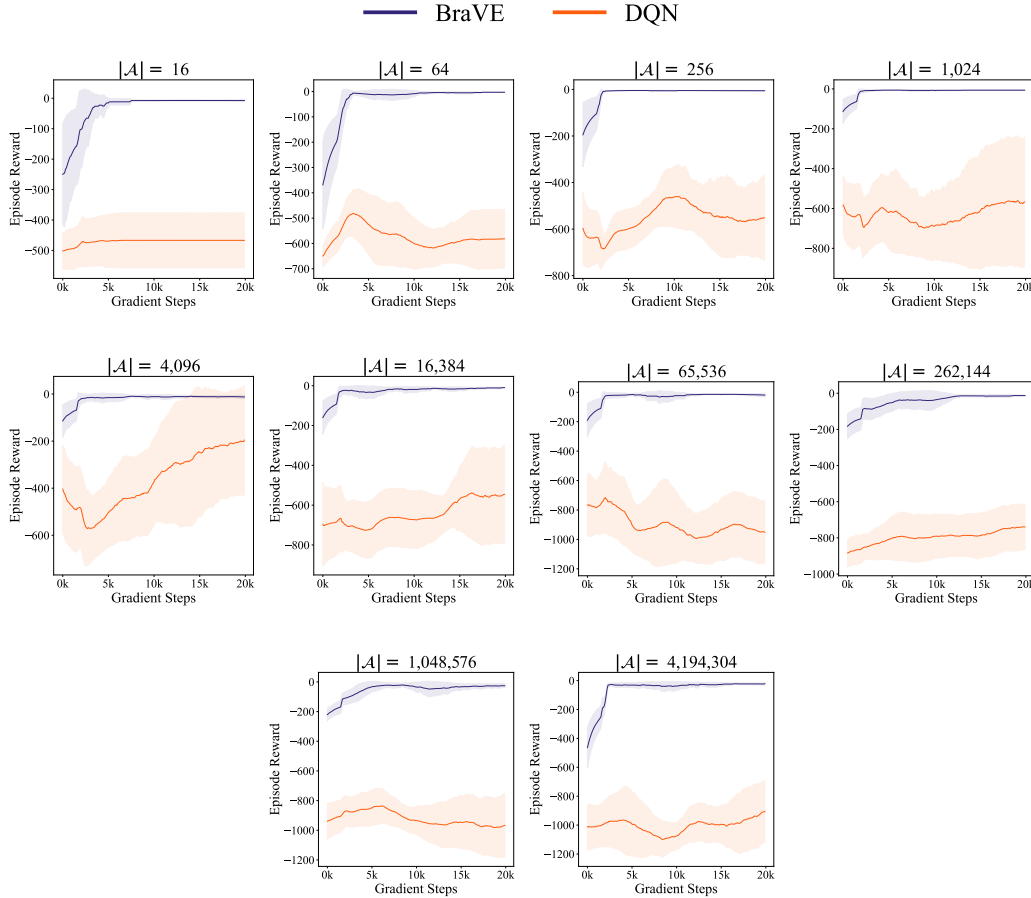


Figure 12: Learning curves for BraVE and a DQN constrained to select actions from  $\mathcal{B}$  and trained with BraVE’s behavior-regularized TD loss (Equation 4) — effectively, BraVE without tree-based action selection or branch value propagation.

Although the DQN is trained with the same behavior-regularized TD loss as BraVE and is restricted to selecting actions in  $\mathcal{B}$ , it fails to learn an effective policy. This suggests that the DQN struggles to capture sub-action dependencies, particularly in large action spaces. For example, in the 11-D environment, it must evaluate all 8,927 unique actions in  $\mathcal{B}$  simultaneously. BraVE mitigates this complexity by organizing the action space as a tree, reducing the number of required predictions to a small subset of Q-values at each timestep.

## D.4 Beam Width

Because beam search is used only during policy extraction — after value estimates have been learned — it remains independent of the learning process. This decoupling allows for post-training optimization of beam width, provided the environment permits hyperparameter tuning. To evaluate the impact of beam width on both return and computational overhead, we measure return, environment steps per second, and total episode runtime for beam widths ranging from 5 to 500.

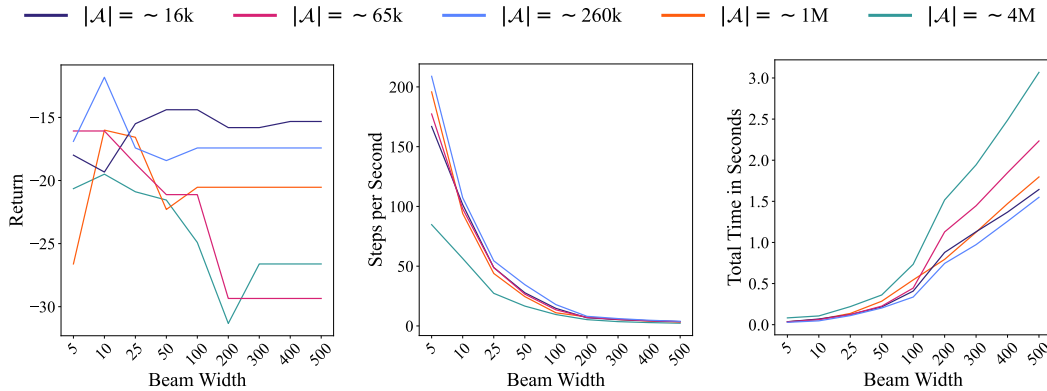


Figure 13: Effect of beam width on return and computational cost, measured in environment steps per second and total episode runtime.

A beam width of 10 is generally sufficient to achieve optimal performance, with little to no improvement from larger values. Furthermore, beam width has negligible practical impact on runtime: inference times remain well below one second, even for beam widths far exceeding the optimal setting. These results are based on tests conducted on a 10-core CPU with 32 GB of unified memory and no GPU.